Brain Growth Rate Abnormalities Visualized in Adolescents with Autism

Xue Hua,[1] Paul M. Thompson,[1] Alex D. Leow,[1,4] Sarah K. Madsen,[1] Rochelle Caplan,[3] Jeffry R. Alger,[2] Joseph O'Neill,[3] Kishori Joshi,[3] Susan L. Smalley,[3] Arthur W. Toga,[1] and Jennifer G. Levitt[3]*

[1]*Laboratory of Neuro Imaging, University of California Los Angeles School of Medicine, Los Angeles, California*
[2]*Ahmanson-Lovelace Brain Mapping Center, Department of Neurology, University of California Los Angeles School of Medicine, Los Angeles, California*
[3]*Department of Psychiatry and Biobehavioral Sciences, Division of Child Psychiatry, University of California Los Angeles School of Medicine, Los Angeles, California*
[4]*Semel Institute of Neuroscience, University of California Los Angeles School of Medicine, Los Angeles, California*

Abstract: Autism spectrum disorder is a heterogeneous disorder of brain development with wide ranging cognitive deficits. Typically diagnosed before age 3, autism spectrum disorder is behaviorally defined but patients are thought to have protracted alterations in brain maturation. With longitudinal magnetic resonance imaging (MRI), we mapped an anomalous developmental trajectory of the brains of autistic compared with those of typically developing children and adolescents. Using tensor-based morphometry, we created 3D maps visualizing regional tissue growth rates based on longitudinal brain MRI scans of 13 autistic and seven typically developing boys (mean age/interscan interval: autism 12.0 ± 2.3 years/2.9 ± 0.9 years; control 12.3 ± 2.4/2.8 ± 0.8). The typically developing boys demonstrated strong whole brain white matter growth during this period, but the autistic boys showed abnormally slowed white matter development ($P = 0.03$, corrected), especially in the parietal ($P = 0.008$), temporal ($P = 0.03$), and occipital lobes ($P = 0.02$). We also visualized abnormal overgrowth in autism in gray matter structures such as the putamen and anterior cingulate cortex. Our findings reveal aberrant growth rates in brain regions implicated in social impairment, communication deficits and repetitive behaviors in autism, suggesting that growth rate abnormalities persist into adolescence. Tensor-based morphometry revealed persisting growth rate anomalies long after diagnosis, which has implications for evaluation of therapeutic effects. *Hum Brain Mapp 00:000–000, 2011.*

Additional Supporting Information may be found in the online version of this article

Contract grant sponsor: National Institutes of Health (NIH) through the NIH Roadmap for Medical Research; Contract grant number: U54 RR021813; Contract grant sponsor: National Center for Research Resources (NCRR), a component of the NIH; Contract grant number: P41 RR013642 and M01 RR000865; Contract grant sponsor: National Alliance for Autism Research (NAAR); Contract grant number: grants 01082668; Contract grant sponsor: National Institute of Mental Health (NIMH); Contract grant number: 5K08 MH01385 and MH067187; Contract grant sponsor: National Institute of Neurological Disorders and Stroke (NINDS); Contract grant number: 5R01 NS046018 and NS32070; Contract grant sponsor: National Institute of Biomedical Imaging and Bioengineering (NIBIB); Contract grant number: R01 EB007813, R01 EB008281, R01 EB008432; Contract grant sponsor: National Institute of Child Health and Human Development (NICHHD); Contract grant number: R01 HD050735; Contract grant sponsor: National Institute on Aging (NIA); Contract grant number: R01 AG020098.

*Correspondence to: Jennifer G. Levitt, UCLA Department of Psychiatry & Biobehavioral Sciences, BOX 951759, 760 Westwood Plaza, 47-417C Semel Institute, Los Angeles, CA 90095-1759. E-mail: jlevitt@mednet.ucla.edu

Received for publication 12 August 2010; accepted 27 July 2011

DOI: 10.1002/hbm.21441

Published online in Wiley Online Library (wileyonlinelibrary.com).

Key words: autism spectrum disorder; longitudinal; MRI; tensor-based morphometry; development; white matter

INTRODUCTION

Autism spectrum disorder is a complex neurodevelopmental disorder with a lifelong impact. It affects approximately one in 110 children, with a male-to-female ratio of 4.5:1, according to a recent Center for Disease Control and Prevention survey [CDC 2009]. Autism is clinically characterized by behavioral abnormalities including social deficits, language impairments, and restricted or stereotyped behaviors, present by age 3 or earlier [Kanner 1943; Lord et al. 2000a].

During typical development, the brain undergoes a highly dynamic process of dendritic branching, synaptic pruning, and myelination, which continues into adolescence and adulthood [Giedd et al. 1999; Gogtay et al. 2004; Knickmeyer et al. 2008; Sowell et al. 1999; Sowell et al. 2004]. In contrast, the brains of at least some autistic children are hypothesized to undergo accelerated brain growth before age 2 followed by a premature slowing of growth [Courchesne 2004; Courchesne et al. 2004]. This anomalous trend has been found using both traditional head circumference measurements [Courchesne et al. 2003] and magnetic resonance imaging (MRI) of brain volume [Brambilla et al. 2003; Courchesne et al. 2001; Sparks et al. 2002]. As most of the autism studies focused on very early stages of development, the trend of brain growth later in life remains unidentified. In addition, brain volume changes in cross-sectional studies do not necessarily imply accelerated or decelerated growth, which can only be conclusively established with a longitudinal design [Amaral et al. 2008; Brambilla et al. 2003].

MRI is a safe, noninvasive method to investigate brain morphology in children and adolescents [Brambilla et al. 2003; Eliez and Reiss 2000]. Tensor-based morphometry (TBM) is an automated image analysis technique that identifies regional structural differences between scans [Gogtay et al. 2008; Thompson et al. 2000]. In longitudinal studies, a deformation field is obtained by nonlinearly registering the MRI scans of the same subject acquired at different times. Then a tensor field, the Jacobian matrix, is calculated from the gradient of the deformation field to characterize brain change [Ashburner and Friston, 2003]. A color-coded Jacobian determinant map represents volume loss or gain at each voxel [Ashburner and Friston, 2003; Chung et al. 2001; Freeborough and Fox 1998; Riddle et al. 2004; Toga 1999]. TBM offers a detailed 3D mapping of structural changes in cortical and subcortical tissues, including cerebral white matter and deep brain nuclei.

In this study, we evaluated 13 autistic and seven typically developing boys, over a period of 2–6 years. We hypothesized that children with autism undergo abnormal brain development compared with healthy kids, evidenced by structural MRI. We computed 3D Jacobian maps to estimate the rate of local tissue change between baseline and follow-up for each subject. By comparing the patient and control groups, we detected an abnormal slowdown of cerebral white matter development, as well as overgrowth of deep gray matter structures including the putamen (PT) and anterior cingulate cortex (ACC). For the first time, we report ongoing changes in the autistic brain during adolescence, providing direct evidence for abnormalities of brain maturation after early childhood. Accurate tracking of late abnormalities offers an opportunity to assess the effects of therapy and may assist in finding genes associated with these deficits.

Abbreviations

ACC	anterior cingulate cortex
ADI-R	Autism Diagnostic Interview Revised
ADOS	Autism Diagnostic Observation Schedule
FDR	false discovery rate
FFT	Fast Fourier Transform
FL	frontal lobe
FSIQ	full-scale intelligence quotient
ICBM	International Consortium for Brain Mapping
MDT	minimal deformation target
MRI	magnetic resonance imaging
PIQ	performance intelligence quotient
PT	putamen
ROI	regions of interest
TBM	tensor-based morphometry
VIQ	verbal intelligence quotient

MATERIALS AND METHODS

Subjects

Thirteen autistic and seven typically developing children and adolescents aged 6 to 17 participated in this study (Table I). All subjects were males. Each subject received two high-resolution 3D MRI scans with an average interscan interval of 2.9 ± 0.9 years. The average age represents the midpoint age between the two scan dates, which was 12.0 ± 2.3 years for the autistic group and 12.3 ± 2.4 years for the control group. There was no significant age difference between the two groups ($P = 0.77$). The full data for the ages of each subject at the times of the first and second scans is provided in the Supporting Information (Table IS).

Inclusion criteria for the autistic subjects were a DSM-IV (American Psychiatric Association, 1994) diagnosis of autism or pervasive developmental disorder, absence of medical or neurological illness, and performance intelligence quotient (PIQ) >70. Diagnoses were based upon

TABLE I. Age and interscan interval

	Control ($n = 7$, male)				Autism ($n = 13$, male)			
	Age (years)				Age (years)			
	1st scan	2nd scan	Average	Interval	1st scan	2nd scan	Average	Interval
Mean	10.9	13.7	12.3	2.8	10.5	13.4	12.0	2.9
SD	2.3	2.6	2.4	0.8	2.3	2.4	2.3	0.9
Min	6.5	8.7	7.6	1.9	7.5	9.6	8.5	2.1
Max	13.4	16.2	14.8	4.4	13.7	16.7	15.2	5.7

structured interviews using the Autism Diagnostic Interview Revised (ADI-R) [Lord et al. 1994] and the Autism Diagnostic Observation Schedule (ADOS) [Lord et al. 1999]. The ADI-R, a semi-structured interview administered to the primary caregivers, and the ADOS are widely used in the diagnosis of autism. The ADI-R has excellent reliability and validity [Le Couteur et al. 1989], as does the ADOS-G [Lord et al. 2000b]. All subjects in the autistic group met criteria for autism based on ADI-R and ADOS scores (ADOS-communication: 4.7 ± 2.1, ADOS-qualitative impairments in reciprocal social interaction: 9.7 ± 2.0, ADOS-play or imagination/creativity: 1.0 ± 0.6, ADOS-stereotyped behaviors, and restricted interests: 0.9 ± 1.1) administered by qualified raters (J.L., S.S.). Four of the autistic subjects were on medications at the first visit: one patient on clonidine and dexadrine at the first visit remained on these medications at the second visit; one patient on methylphenidate remained on this medication at the second visit; one subject on methylphenidate and Risperidone at the first visit returned on mixed salts and Risperidone at the second visit; and one on Sertraline at the first visit returned on no psychopharmacologic medications at the second visit. Additionally, one patient on no medications at the first visit returned on paroxetine at the second visit. Subjects were asked to remain free of stimulant medications for 24 hours prior to the scan, but other medications were not suspended. Because of the small number of subjects in the study, it was not plausible to covary for medication use. The full-scale (FSIQ), verbal (VIQ), and PIQ scores were evaluated according to the Wechsler Intelligence Scale for Children-Third Edition [Wechsler 1991]. The mean FSIQ/VIQ/PIQ of the patients was 98/95/102 [standard deviation (SD) = 23/24/21] at baseline and 101/100/100 (SD = 22/24/21) at follow-up. There was one missing data point of IQ at baseline and at follow-up, respectively.

Control children were recruited from public and private schools in the community. Controls were screened for neurological, psychiatric, language, or hearing disorders by clinical interview, developmental history and K-SADS-PL [Kaufman et al. 1997] interviews with the parents. The K-SADS-PL is a highly reliable structured interview used to assess a wide range of psychiatric disorders according to either DSM-III-R or DSM-IV criteria. We excluded children from the control sample if they met criteria for any lifetime significant medical disorder or Axis I mental disorder. The mean FSIQ/VIQ/PIQ of the control group was 118/120/112 (SD = 13/15/10) at baseline and 118/122/118 (SD = 8/8/11) at follow-up. The FSIQ was significantly different between the autistic and control groups at baseline ($P = 0.03$) and follow-up ($P = 0.03$).

All subjects were recruited as part of an ongoing neurodevelopmental project at the University of California, Los Angeles, approved by the University of California, Los Angeles Human Subjects Protection committee. All parents of subjects provided written informed consent for participation and, where possible, subjects provided assent.

MRI Acquisition

All subjects completed MRI scans on the same 1.5 Tesla GE Signa magnetic resonance imaging scanner (GE Medical Systems, Milwaukee, WI). High-resolution 3D T1-weighted spoiled grass sequences were obtained using the following imaging acquisition protocol: a sagittal plane acquisition with slice thickness of 1.2 mm, repetition time of 14.6, echo time of 3.3, flip angle of 35°, an acquisition matrix of 256 × 192, field of view of 24 cm and two excitations.

Image Preprocessing

Scalp and other non-brain tissues were removed using an automated program, Brain Surface Extractor, from BrainSuite [Shattuck and Leahy 2002], followed by manual editing in all sagittal planes to lower the segmentation error caused by similar image intensities for brain (i.e., gray matter, white matter, and cerebrospinal fluid) and non-brain tissues. A three-dimensional radio frequency bias field correction algorithm (N3) was applied to reduce intensity inhomogeneity in MRI images caused by nonuniformities in the radio frequency receiver coils [Sled et al. 1998]. A prior validation study demonstrated the improved longitudinal stability of TBM with scans acquired using spoiled grass sequence followed by N3 correction [Leow et al. 2006].

To account for global differences in positioning among individual brains, all scans were rigidly aligned to the

ICBM53 standard brain, a stereotaxic space defined by the International Consortium for Brain Mapping (ICBM) [Mazziotta et al. 2001]. To linearly align the scans to ICBM53 brain, each follow-up scan was linearly registered to its baseline scan with 6-parameter (6p) affine transformation, then both scans were registered to ICBM53 using the same 9-parameter (9p) transformation, with mutual information as a similarity measure [Maes et al. 1997]. In the 9p linear registration to the ICBM53 brain, all MRI images were resampled into an isotropic matrix of 199 voxels in x-, y-, and z dimensions with each voxel interpolated to the size of $1 \times 1 \times 1$ mm. The quality of linear registration was visually inspected by using a 3D visualization tool called REGISTER, which automatically overlays the arbitrary slice geometry of each scan pair in ICBM53 space [MacDonald 1993]. All scans had satisfactory results for linear registration without noticeable distortion or mismatch.

Minimal Deformation Target

Prior studies have suggested that inter-subject registration of MRI scans from children is improved if a specially constructed image—a custom-made group-average template—is used as a target [Wilke et al. 2008; Wilke et al. 2002]. We constructed a minimal deformation target (MDT) using the baseline scans of all subject included in the study [Good et al. 2001; Kochunov et al. 2002; Kovacevic et al. 2005; Woods et al. 1998]. Steps for creating a MDT are detailed in prior publications [Hua et al. 2008; Hua et al. 2009]. Briefly, an affine average image was created from baseline images after nine-parameter affine registration to ICBM53. Each scan was then nonlinearly registered to the affine average template using a nonlinear inverse-consistent elastic intensity-based registration algorithm [Leow et al. 2005; Thompson et al. 2000; Wells et al. 1996]. The deformation field was determined by maximizing the mutual information of the image intensities and minimizing the elastic energy of the deformation. A multiresolution scheme was used. It began with a Fast Fourier Transform (FFT) resolution of $32 \times 32 \times 32$ followed by $64 \times 64 \times 64$, which corresponds to an effective voxel size of 30 mm^3 (199 mm/64 = 3.1 mm), with 300 iterations at each resolution. A nonlinear average was computed by voxel-wise averaging the intensities of the 20 images (13 autistics + 7 controls) that had been nonlinearly registered to the affine average template. Finally, the MDT was created by adjusting the nonlinear average with inverse geometric centering of the displacement fields [Kochunov et al. 2005; Kochunov et al. 2002]. The MDT was subsequently used as the target for inter-subject registration.

Jacobian Maps Construction

We used the same nonlinear registration algorithm, as used in creating the MDT, to spatially adjust for both intra- and inter-subject shape differences. The deformation field obtained from intrasubject scan pairs $U_{Intra}{}^{Dn}$ (D, diagnosis; "A" as autism and "C" as control; n, subject index) represents developmental changes in an individual brain. A tissue change map was derived from the deformation field obtained by warping the follow-up scan of each subject to its baseline scan. Each map was adjusted using its corresponding interscan interval to create an annualized Jacobian map that represents the average change per year, or growth rate. The intersubject registration $U_{Inter}{}^{Dn}$ encodes the anatomical variance between individual brains. To align individual Jacobian maps to a common stereotactic space, the initial scan of each subject was nonlinearly aligned to the geometry of the MDT template (32 FFT $\times$300 iterations; 64 FFT $\times$300 iterations). The inter-subject displacement vector field $U_{Inter}{}^{Dn} = (u_x, u_y, u_z)$, was then applied to transform the individual Jacobian growth map J^{Dn}. $J^{Dn}{}_s$ (s, standard space) symbolizes individual Jacobian maps aligned in the standard space defined by the MDT template. Spatial normalization across different brains is a computationally intensive step, but it reduces inter-individual variance in brain anatomy enabling regional comparisons and group analyses. See Fig. 1 for a diagram of the design. All group comparisons and statistical analyses are based on the annualized Jacobian maps (tissue change per year) in the standard space.

The image processing steps were executed using the LONI Pipeline Processing Environment, which streamlines the process and allows parallelization of multiple tasks [Rex et al. 2003].

Regions of Interest

Regions of interest (ROIs) were delineated on the MDT template by a trained anatomist (S.M.). Lobar masks, for the frontal (FL), parietal, temporal, and occipital lobes (left, right, both sides), were manually created on the MDT by a trained expert (S.M.) (Fig. 2). The detailed protocol is available on the LONI Research Protocols website: (http://cms.loni.ucla.edu/ncrr/protocols.aspx?id = 1482). An ROI of the white matter was generated automatically using the tissue classification tool in BrainSuite [Shattuck and Leahy 2002]. The ROIs were also combined to create additional lobe-specific white matter masks.

Statistical Analyses

We used nonparametric methods to estimate the sample mean and standard error of voxel-wise statistical testing. To build average tissue change maps and assess statistical significance at each voxel, the Jacobian maps were analyzed using the bootstrap method [Efron and Tibshirani 1986; Efron and Tibshirani 1993]. The bootstrap was performed for the autism and control groups separately. Using the autism group as an example, we generated 1,000 independent bootstrap samples, each of size $n = 13$ with replacements from the 13 individual Jacobian maps.

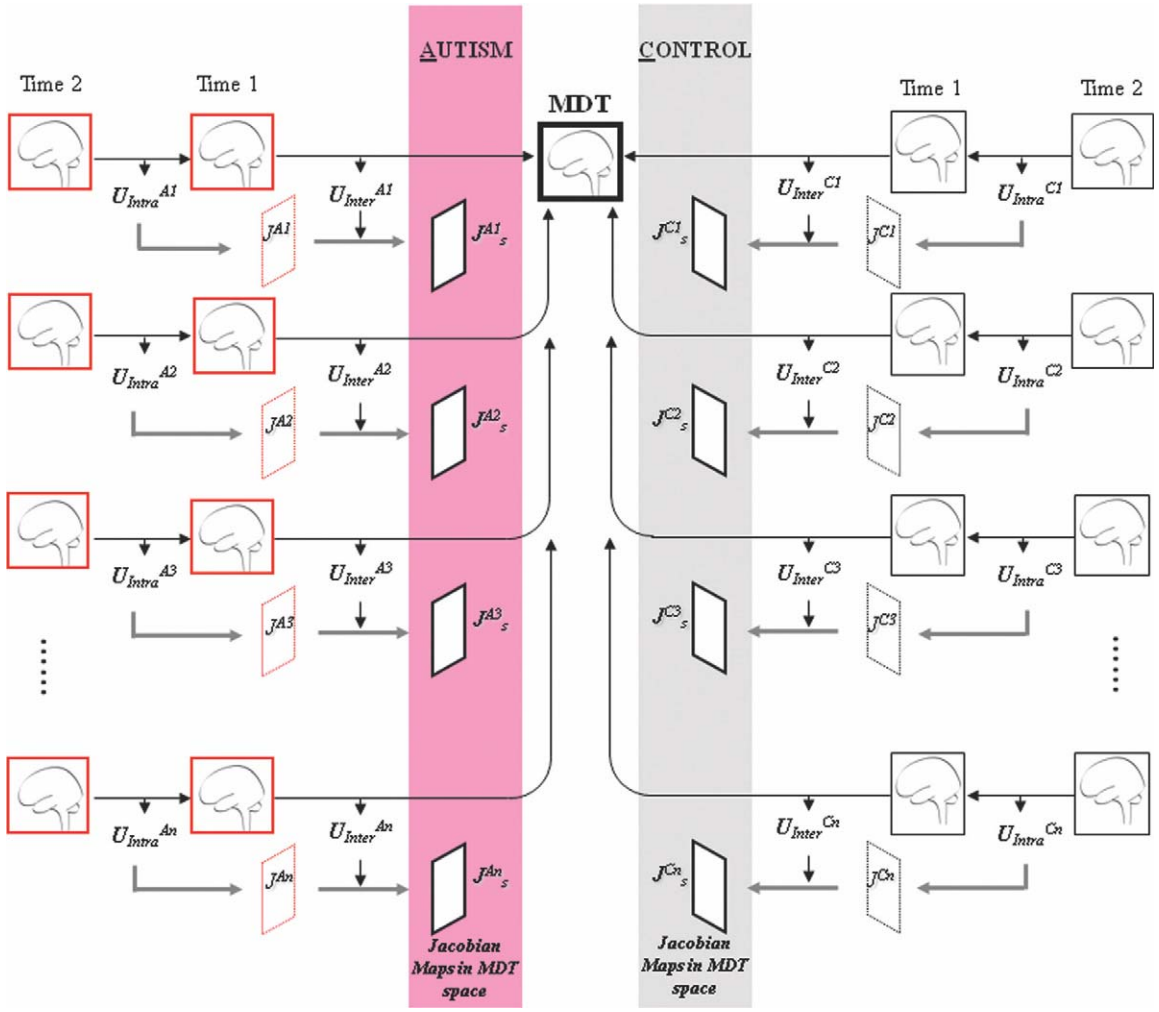

Figure 1.

Diagram of the study design. Individual Jacobian maps J^{Dn} (D, diagnosis; "A" as autism, and "C" as control; n, subject index) are derived from the deformation matrix $U_{Intra}{}^{Dn}$, which is obtained by iteratively deforming the follow-up scan (Time 2) to the initial scan (Time 1) of the same subject. Variance across individual brains is modeled by using an inter-subject deformation field, $U_{Inter}{}^{Dn}$. The displacement vector field $U_{Inter}{}^{Dn} = (u_x, u_y, u_z)$ is applied to transform the Jacobian growth map of each subject (J^{Dn}) to the detailed brain anatomy defined by the MDT template. $J^{Dn}{}_s$ (s, standard space) represents the individual Jacobian map in the standard space. [Color figure can be viewed in the online issue, which is available at wileyonlinelibrary.com.]

The bootstrap estimate of standard error is the SD of the bootstrap replications [Efron and Tibshirani 1993]. Using the same protocol, the voxel-wise mean and standard error were estimated for the control group ($n = 7$). The mean difference map (autism minus control) was computed to display the autistic subject's deviation from typical development. At each voxel, a two-sample t test was carried out based on the bootstrap sample mean and bootstrap estimate of standard error for the two groups.

Permutation tests were implemented to assess the overall significance of group difference inside each ROI, corrected for multiple comparisons [Nichols and Holmes 2002]. The null hypothesis is that, for each ROI, there is no differential developmental change in terms of tissue growth or loss between the two groups. Under the null hypothesis, the group labels—autism and control—are interchangeable. At each permutation, group labels were randomly permuted and voxels with $P \leq 0.01$ (uncorrected) were identified from a two-sample t test. After 10,000 randomized tests, a ratio was calculated describing what fraction of time an effect of similar or greater magnitude than the real effect occurs in the random assignments. This ratio serves as an overall estimate of significance for the maps (corrected for multiple comparisons) [Nichols and Holmes 2002]. Positive growth signals and negative tissue loss were assessed separately in each ROI.

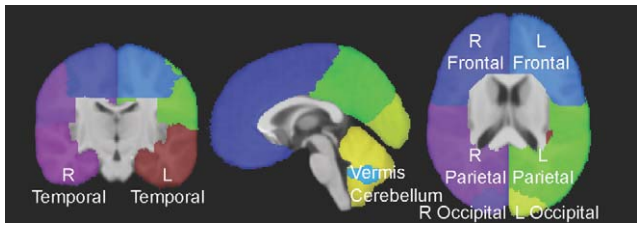

Figure 2.
Lobar masks were manually created on the MDT, designating left (L) and right (R) frontal, parietal, temporal, and occipital lobes. [Color figure can be viewed in the online issue, which is available at wileyonlinelibrary.com.]

Using the general linear model, correlations were assessed between brain growth rates and (1) mean IQ (average IQ at first and second scans); (2) change of IQ (IQ at second scan minus IQ at first scan), at each voxel within the brain, in each group independently and in the combined group with both autism and control subjects. These correlations were subsequently evaluated by cumulative distribution functions to correct for multiple comparisons using the false discovery rate (FDR) [Benjamini and Hochberg 1995], inside the whole brain, white matter, and gray matter. A significant correlation is declared if a FDR critical $P > 0$ can be found to control for FDR at less than 5% level [Hua et al. 2008; Hua et al. 2010; Morra et al. 2008].

RESULTS

IQ and Brain Growth

The rates of brain growth (Jacobian values) at each voxel were tested for correlation with mean IQ and change of IQ between the two scans, in each group independently and in the combined group with both autism and control subjects. There was no significant correlation between growth rates and mean IQ or change of IQ (for FSIQ, VIQ, and PIQ) inside the whole brain, gray matter, or white matter, after correction for multiple comparisons. We therefore excluded IQ from subsequent analyses.

Individual Tissue Change Maps

To illustrate how TBM can map anatomical brain development, we show the individual tissue change maps for an 11-year-old healthy child (initial scan at age 10) and an autistic subject of similar age (Fig. 3). The Jacobian map represents the amount of tissue change, as a percentage, over a period specified by the scan interval, with the hot and cold colors representing local tissue expansion and atrophy, respectively. In the following group analysis, the Jacobian maps were adjusted using their corresponding scan intervals to illustrate average change per year.

The selected control subject has active growth in multiple white matter regions—a developmental trend typically observed in childhood and adolescence [Giedd et al. 1999; Gogtay et al. 2008; Hua et al. 2009]. In contrast, the 11-year-old autistic child displays negligible changes in white matter, in regions showing strong growth in the control subject (e.g., the frontal and parietal lobes). The individual Jacobian maps visualize detailed growth patterns that are later confirmed by group analysis.

Mean Jacobian Maps and Group Comparison

Fig. 4 shows three sets of tri-planar views of the MDT, the annual mean Jacobian map of the control group, the annual mean Jacobian map of the autistic group, the average group difference map and the map of P values for the between-group comparison. All maps were computed using the bootstrap method to get the correct empirical null distribution at each voxel, as detailed in the methods section. Compared with typical development, the autism

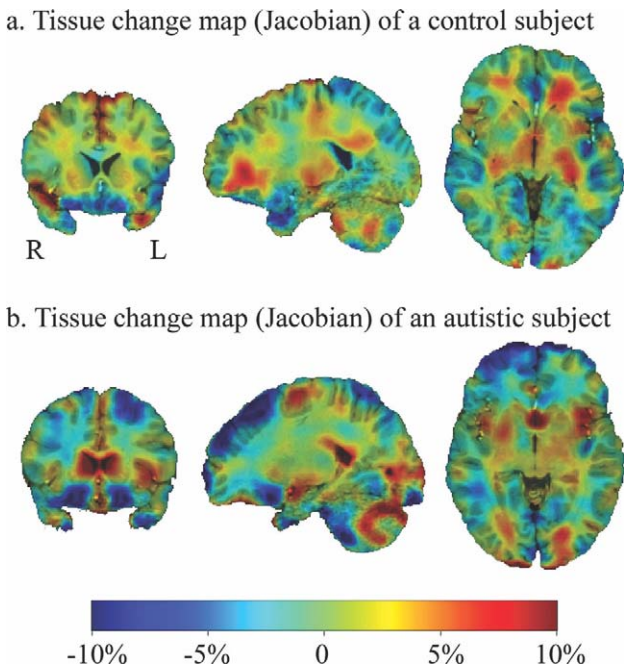

Figure 3.
Individual tissue change (Jacobian) maps of an 11-year-old typically developing boy (scan interval: 2.2 years) (a) and a similarly aged autistic boy (scan interval: 2.9 years) (b). The initial scan was conducted around 10 years of age for each subject. The Jacobian map illustrates the overall percentage of tissue change during the scan interval. The color coded Jacobian map is displayed over the structural MRI image, with the hot and cold colors representing local tissue expansion and atrophy, respectively. Standard radiologic convention is used to display the images. [Color figure can be viewed in the online issue, which is available at wileyonlinelibrary.com.]

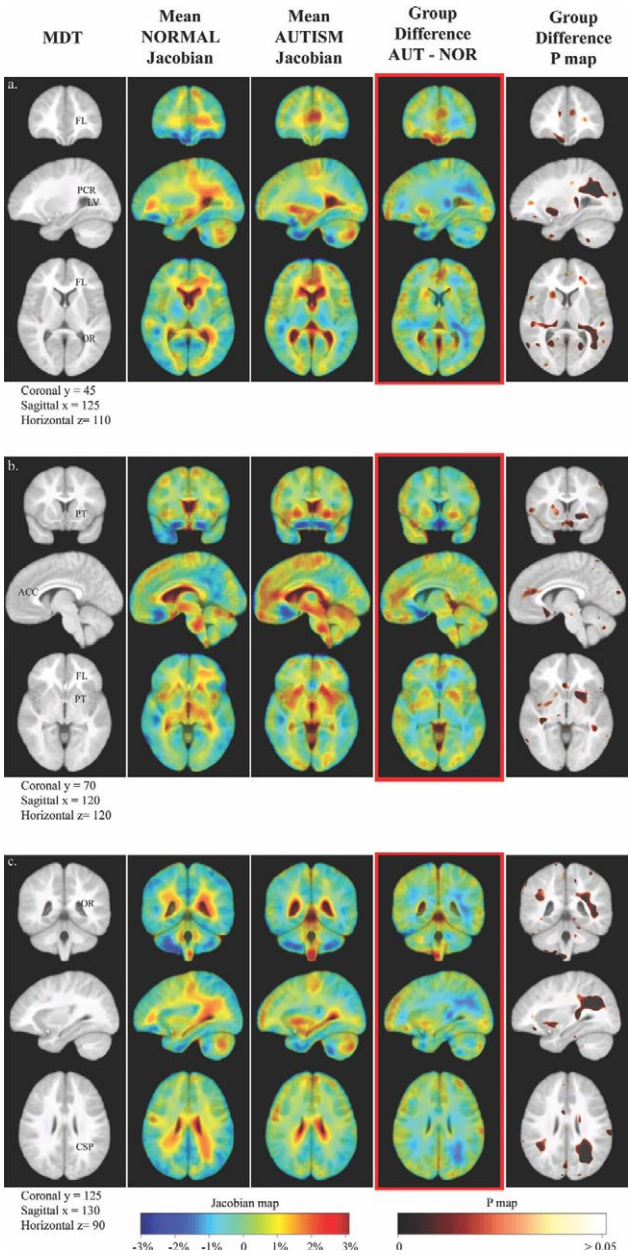

Figure 4.

Annual tissue growth rates (percentage of tissue change per year) mapped in the control group, the autistic group, and the difference in growth rates between the two groups. Each set of tri-planar images is chosen to show anatomical regions with considerable deviation from typical development. Compared with the control group, the autistic group exhibits abnormal growth patterns in several white and gray matter structures. ACC, anterior cingulate cortex; CSP, *centrum semiovale* in the dorsal core of the parietal lobe; FL, frontal lobe; LV, lateral ventricle (posterior horn); OR, optic radiation; PCR, posterior *corona radiata*; PT, putamen. [Color figure can be viewed in the online issue, which is available at wileyonlinelibrary.com.]

group map exhibits a reduced growth rate for cerebral white matter (Fig. 4) in multiple regions. (1) The frontal lobe: the corticopontine tract, the corpus callosum, and the anterior thalamic radiation (Fig. 4a,b). (2) The parietal lobe: the posterior corona radiata including the corticopontine tract, the inferior longitudinal fasciculus, the posterior thalamic radiation, and the corpus callosum (Fig. 4a); and the centrum semiovale in the dorsal core of the parietal lobe, a region that that may include fibers from the superior longitudinal fasciculus, the corticopontine tract, the inferior fronto-occipital fasciculus, and the inferior longitudinal fasciculus (Fig. 4c). (3) The temporal lobe: the sagittal stratum which is a large white matter tract composed of fibers from the corticopontine tract, the posterior thalamic radiation (including the fibers from the optic radiation), the inferior fronto-occipital fasciculus, and the inferior longitudinal fasciculus (Fig. 4a,c). (4) The occipital lobe: the optic radiation as part of the sagittal stratum (Fig. 4a). The identification of these white matter tracts is based on the MRI atlas of the human brain [Mori et al. 2005]. In gray matter, Fig. 4b suggests a possible overgrowth of PT and ACC in autism.

Permutation Tests

A permutation test was used to assess the overall significance of differential brain development within each ROI. 10,000 randomization tests were conducted and confirmed the trend of arrested white matter development in autism when compared with the controls (Table II). Frontal white matter displayed slower regional growth (Fig. 4) but this did not reach overall significance after correction for multiple comparisons (Table II). The abnormally slower white matter growth was more pronounced in the left hemisphere than the right, as visualized in the maps (Fig. 4) and indicated by the permutation P values. To analyze this further, we conducted a posthoc hemispheric asymmetry test for white matter growth rates for each group independently. A mirror image of each individual's Jacobian map was created by reflecting the map with respect to its midsagittal plane. Permutation tests based on paired two-sample t tests were then performed to assess whether

TABLE II. *P* values of abnormally slowed white matter development in autism compared with typically developing children and adolescents, corrected for multiple comparisons using permutation tests

	Whole brain	Frontal	Parietal	Temporal	Occipital
Left	0.01*	0.3	0.0009**	0.04*	0.01*
Right	0.1	0.6	0.08	0.04*	0.1
Left + right	0.03*	0.5	0.008**	0.03*	0.02*

*$P < 0.05$.
**$P < 0.01$.

regional growth rate was significantly asymmetrical, while correcting for multiple comparisons. These analyses did not detect a statistically significant asymmetry for white matter growth rates in either the autism or the control group (all corrected $P > 0.05$).

DISCUSSION

Although autism is typically diagnosed before 3 years of age, our study suggests ongoing developmental delays in the autistic brain during adolescence, a critical period to establish personal identity and develop/refine emotional and social skills. In cross-sectional MRI studies of autism, one of the most consistent findings is an abnormal brain volume enlargement in early childhood [Courchesne et al. 2003; Courchesne et al. 2001; Hazlett et al. 2005; Sparks et al. 2002]. With a longitudinal study design, we offer direct evidence for anomalous development of the autistic brain that persists from late childhood to adolescence. We found decelerated white matter growth in the frontal, temporal, parietal, and occipital lobes, as well as abnormally accelerated gray matter expansion in the PT and ACC. Regions showing aberrant growth rates largely correspond to brain areas implicated in core behavioral characteristics of autism: social impairment, communication deficits and repetitive behaviors [Amaral et al. 2008]. The significance of deceleration vs. acceleration is unclear and likely complex, resulting possibly from interactions between factors such as understimulated or insufficiently inhibited tissue growth, history of exercise of regional function, competition between tracts or regions for intracranial space, and compensatory processes. These abnormal changes may offer a quantitative method to assess the impact on the brain of educational interventions in later life for autistic individuals.

Brain Volume

Despite findings of early brain enlargement in autism in several studies [Courchesne 2004; Courchesne et al. 2003; Sparks et al. 2002], the difference in brain size might not persist into adolescence and adulthood. Several studies detected no significant brain volume difference with respect to normals [Courchesne et al. 2001; Hardan et al. 2009; Herbert et al. 2003; Kates et al. 2004], while others found a larger brain size in autistic subjects in adolescence [Piven et al. 1996; Piven et al. 1995], or regional structural brain differences (Hyde et al. 2009). Moreover, the degree to which gray and/or white matter is responsible for such brain abnormalities remains a subject of investigation. A hypothesis first postulated by Herbert et al. [2003] and supported by other studies [Courchesne et al. 2001; Hazlett et al. 2005], is that the abnormal brain enlargement observed in children with autism is disproportionately accounted for by an increase in white matter, not gray matter. A recent longitudinal study observed a greater decrease in gray matter in autism, measured by total gray matter volume and cortical thickness at a 30-month interval [Hardan et al. 2009]. The rates of gray matter pruning between autistic and normal, however, did not reach significance after accounting for multiple comparisons, with the exception of changes in occipital cortical thickness. Here, we found a highly significant and widespread reduction of cortical white matter growth in autism in childhood and adolescence, which may counterbalance the effects of early brain overgrowth together with changes in gray matter, decreasing the disparity in brain volume relative to control subjects.

A Theory of Under Connectivity

A promising theory proposes that autism is not simply associated with regional brain deficits, but also involves deficiencies in cortical networks, which results in functional under-connectivity between cortical regions [Belmonte et al. 2004; Frith 1989]. Functional MRI studies have examined autistic subjects' difficulties in integrating complex information (e.g., language, social cognition, and problem solving) with relative conservation of the ability to analyze individual features [Bachevalier and Loveland 2006; Barnea-Goraly et al. 2004; Castelli et al. 2002; Herbert et al. 2004; Just et al. 2007; Just et al. 2004; Koshino et al. 2005]. A neural network model proposes that local over-connectivity and long range under-connectivity may cause a reduction in information transfer in autism [Belmonte et al. 2004; Herbert et al. 2004; Just et al. 2004]. Here, we identified abnormally slowed white matter development in brain regions carrying long-range fibers connecting functional regions important for higher-order functions such as language and social behaviors. However, with T1-weighted MRI scans, we could not identify the source of this white matter impairment. Whether it involves a reduced number of fibers, a change in myelination, or other factors that might affect connectivity, remains an unanswered question.

Regional Brain Deficits in Autism

Some structural MRI studies found enlarged parietal lobe volume in juvenile and young male adults with autism, which may indicate developmental abnormalities in these regions [Carper et al. 2002; Piven et al. 1996]. Our results demonstrate growth rate slowing that is most striking in the left parietal lobe, whereas the right parietal lobe is relatively unaffected (Table II). These findings may be associated with impairments in language development. Compared with typical development, the autism group exhibits a reduced growth rate in the optic radiations. This finding is consistent with two recent diffusion tensor imaging studies on autistic children, which identified significant reduction of fractional anisotropy in the left optic radiations extending into the medial temporal gyrus

(autism group: 14.6 ± 3.4 years, $n = 7$; control group: 13.4 ± 2.8, $n = 9$) [Barnea-Goraly et al. 2004], and in the posterior limbs of the right and left internal capsules consisting of the optic radiations (autism group: 9.5 ± 1.8 years, $n = 8$; control group: 9.6 ± 1.4, $n = 8$) [Brito et al. 2009], in autistic children compared with healthy controls. There were some clusters of significant difference in the cerebellum but these findings did not survive correction for multiple comparisons. A growing number of publications have provided evidence for a cerebellar involvement in autism though the direction of effects is inconsistent [Akshoomoff et al. 2004; Carper and Courchesne 2000; Courchesne et al. 2001; Herbert et al. 2003; Hodge et al. 2010; Kaufmann et al. 2003; Levitt et al. 1999; Scott et al. 2009; Sivaswamy et al. 2010; Sparks et al. 2002; Webb et al. 2009]. We identified a developmental abnormality in autism; however, with the current sample size, we lack sufficient statistical power to establish solid evidence for cerebellar deficits.

Interpretation of Statistical Results

Bootstrap avoids inference based on parametric assumptions but the *P* maps in Figure 4 were not corrected for multiple comparisons. They were used to illustrate regional group difference at each voxel without controlling for cluster size. We then used permutation tests to assess the overall significance of group difference inside each ROI, corrected for multiple comparisons; however, it does not provide inference at the voxel level. The uncorrected *P* maps and the permutation *P* values should be interpreted altogether. An assumption made by converting the brain deformation (Jacobian) to an annualized map that represents the average change per year, and by averaging the results from a large range of ages and times between the first and second scans, is that the rate of brain growth is fairly linear. This assumption is approximately true based on a large neuroimaging brain developmental study of healthy children and adolescence [Giedd et al. 1999]. From 6 to 14 years old, the growth rates are roughly linear in the white matter [Giedd et al. 1999]. It would be prudent to model the age effect with more subjects in future studies.

TBM and Partial Volume Effect

TBM is a nonlinear image registration tool that measures brain changes using serial MRI scans. The Jacobian determinants of the deformation map provide 3D visualization of local tissue volume growth or loss. Inference on white matter growth and/or gray matter loss using TBM is based on changes in tissue boundaries or gray/white contrast, which are related to the underlying tissue microstructure. Nevertheless, it does not offer a direct measurement of the true changes in white matter or gray matter integrity. TBM measures are more accurate or less influenced by partial volume effect in deep brain regions (e.g. white matter and subcortical gray matter structures) where entire voxels are filled with only one type of brain tissue. TBM measures of cortical gray matter and periventricular tissue are more prone to partial volume effect, in that a voxel has a mixture of brain and non-brain tissues (meninges, skull, or CSF), or a mixture of two types of brain tissues (gray matter and white matter). It is especially problematic when non-brain tissues are also changing as part of normal development, such as thickening of the skull during adolescence. We therefore manually removed the skulls (skull stripping) to eliminate this complication, though careful interpretation is still necessary at the interface of two types of tissues due to partial volume effect [Hua et al. 2009].

IQ and Brain Growth

We did not find a significant correlation between IQ and brain growth, though we cannot rule out such an association with the relatively small sample size. It is possible that growth trajectories for gray and white matter might differ in higher vs. lower IQ individuals regardless of diagnosis. The best approach is to covary IQ while comparing the autistic and normal growth rates. However, since two subjects had missing IQ measurements, we could not afford to remove additional subjects from the study.

Time Windows for Detection and Intervention

Although it would be ideal to emphasize early detection and intervention in clinical practice for autism, there is a large unmet need to provide treatment opportunities for adolescent and adult patients. Adolescence is a time of continued brain development with dynamic changes in gray and white matter [Giedd et al. 1999; Thompson et al. 2000]. The course of autism in adolescence and adulthood is generally understudied. Many adolescent and adult patients with autism show improvement, reportedly up to complete remission of individual symptoms in 10%–15% of cases, while the others decline [Seltzer et al. 2004]. There exists a large population of adolescents and adults with autism who are "too old" for early intervention. They will be likely joined by more who failed to undergo or respond to early intervention. Thus, there is a strong motivation for post-childhood longitudinal neuroimaging studies of autism such as ours. Investigations of this type offer some potential to uncover mechanisms supporting improvement or worsening of autistic symptoms and thus to inform therapy development.

Limitations

While the longitudinal component strengthens our study, we cannot entirely rule out Type II errors due to lack of power. With a relatively small sample size, we

consider our findings preliminary and a basis for future research. The study demonstrates the ability of TBM to identify regions most strongly showing local tissue changes in development, advancing our understanding of age and disease-related changes in brain morphometry.

Summary and Future Directions

Despite decades of research on autism, little is known about this devastating disorder. Evidence from twin and family studies suggests a genetic contribution to autism [Bailey et al. 1995; Folstein and Rutter 1977; Steffenburg et al. 1989]. Several candidate genes have been proposed, yet consistent findings are still lacking. TBM can produce high-resolution mapping of abnormal brain growth. Features in these growth maps, computed in larger populations, can facilitate genetic studies and provide a potentially useful biological measure for evaluating interventions.

CONCLUSION

These findings reveal abnormal brain growth rates in autism compared with healthy development, providing direct evidence of ongoing developmental deficits in autism during adolescence and childhood, long after definitive diagnosis of autism before or at age 3. TBM tracks 3D profiles of developmental changes in the human brain, and thus provides a useful biological measure of brain morphometry.

REFERENCES

Akshoomoff N, Lord C, Lincoln AJ, Courchesne RY, Carper RA, Townsend J, Courchesne E (2004): Outcome classification of preschool children with autism spectrum disorders using MRI brain measures. J Am Acad Child Adolesc Psychiatry 43:349–357.

Amaral DG, Schumann CM, Nordahl CW (2008): Neuroanatomy of autism. Trends Neurosci 31:137–145.

Ashburner J, Friston KJ (2003): Morphometry. Human Brain Function, 2nd ed. San Diego: Academic Press. pp 707–724.

Bachevalier J, Loveland KA (2006): The orbitofrontal-amygdala circuit and self-regulation of social-emotional behavior in autism. Neurosci Biobehav Rev 30:97–117.

Bailey A, Le Couteur A, Gottesman I, Bolton P, Simonoff E, Yuzda E, Rutter M (1995): Autism as a strongly genetic disorder: Evidence from a British twin study. Psychol Med 25:63–77.

Barnea-Goraly N, Kwon H, Menon V, Eliez S, Lotspeich L, Reiss AL (2004): White matter structure in autism: preliminary Evidence from diffusion tensor imaging. Biol Psychiatry 55:323–326.

Belmonte MK, Allen G, Beckel-Mitchener A, Boulanger LM, Carper RA, Webb SJ (2004): Autism and abnormal development of brain connectivity. J Neurosci 24:9228–9231.

Benjamini Y, Hochberg Y (1995): Controlling the false discovery rate: A practical and powerful approach to multiple testing. J Roy Stat Soc, Ser B 57:289–300.

Brambilla P, Hardan A, di Nemi SU, Perez J, Soares JC, Barale F (2003): Brain anatomy and development in autism: review of structural MRI studies. Brain Res Bull 61:557–569.

Brito AR, Vasconcelos MM, Domingues RC, Hygino da Cruz LC Jr, Rodrigues Lde S, Gasparetto EL, Calcada CA (2009): Diffusion tensor imaging findings in school-aged autistic children. J Neuroimaging 19:337–343.

Carper RA, Courchesne E (2000): Inverse correlation between frontal lobe and cerebellum sizes in children with autism. Brain 123:836–844.

Carper RA, Mosesc P, Tiguea ZD, Courchesne E (2002): Cerebral Lobes in Autism: Early Hyperplasia and Abnormal Age Effects NeuroImage 16:1038–1051.

Castelli F, Frith C, Happe F, Frith U (2002): Autism, Asperger syndrome and brain mechanisms for the attribution of mental states to animated shapes. Brain 125:1839–1849.

CDC (2009): Prevalence of Autism Spectrum Disorders - Autism and Developmental Disabilities Monitoring Network, United States, 2006. In: Surveillance Summaries, December 18, 2009. MMWR 2009;58(SS10):1–20. Available at: http://www.cdc.gov/mmwr/preview/mmwrhtml/ss5810a1.htm.

Chung MK, Worsley KJ, Paus T, Cherif C, Collins DL, Giedd JN, Rapoport JL, Evans AC (2001): A unified statistical approach to deformation-based morphometry. Neuroimage 14:595–606.

Courchesne E, Karns CM, Davis HR, Ziccardi R, Carper RA, Tigue ZD, Chisum HJ, Moses P, Pierce K, Lord C, Lincoln AJ, Pizzo S, Schreibman L, Haas RH, Akshoomoff NA, Courchesne RY (2001): Unusual brain growth patterns in early life in patients with autistic disorder: An MRI study. Neurology 57:245–254.

Courchesne E, Carper R, Akshoomoff N (2003): Evidence of brain overgrowth in the first year of life in autism. JAMA 290:337–344.

Courchesne E (2004): Brain development in autism: Early overgrowth followed by premature arrest of growth. Ment Retard Dev Disabil Res Rev 10:106–111.

Courchesne E, Redcay E, Kennedy DP (2004): The autistic brain: Birth through adulthood. Curr Opin Neurol 17:489–496.

Efron B, Tibshirani R (1986): Bootstrap methods for standard errors, confidence intervals, and other measures of statistical accuracy. Stat Sci 1:54–77.

Efron B, Tibshirani R (1993): An Introduction to the Bootstrap. London: Chapman & Hall.

Eliez S, Reiss AL (2000): MRI neuroimaging of childhood psychiatric disorders: A selective review. J Child Psychol Psychiatry 41:679–694.

Folstein S, Rutter M (1977): Infantile autism: A genetic study of 21 twin pairs. J Child Psychol Psychiatry 18:297–321.

Freeborough PA, Fox NC (1998): Modeling brain deformations in Alzheimer disease by fluid registration of serial 3D MR images. J Comput Assist Tomogr 22:838–843.

Frith U (1989): Autism: explaining the enigma: Oxford: Blackwell.

Giedd JN, Blumenthal J, Jeffries NO, Castellanos FX, Liu H, Zijdenbos A, Paus T, Evans AC, Rapoport JL (1999): Brain development during childhood and adolescence: A longitudinal MRI study. Nat Neurosci 2:861–863.

Gogtay N, Giedd JN, Lusk L, Hayashi KM, Greenstein D, Vaituzis AC, Nugent TF, 3rd,Herman DH, Clasen LS, Toga AW, Rapoport JL, Thompson PM (2004): Dynamic mapping of human cortical development during childhood through early adulthood. Proc Natl Acad Sci U S A 101:8174–8179.

Gogtay N, Lu A, Leow AD, Klunder AD, Lee AD, Chavez A, Greenstein D, Giedd JN, Toga AW, Rapoport JL, Thompson PM (2008): Three-dimensional brain growth abnormalities in

childhood-onset schizophrenia visualized by using tensor-based morphometry. Proc Natl Acad Sci U S A 105:15979–15984.

Good CD, Johnsrude IS, Ashburner J, Henson RN, Friston KJ, Frackowiak RS (2001): A voxel-based morphometric study of ageing in 465 normal adult human brains. Neuroimage 14(1 Pt 1):21–36.

Hardan AY, Libove RA, Keshavan MS, Melhem NM, Minshew NJ (2009): A preliminary longitudinal magnetic resonance imaging study of brain volume and cortical thickness in autism. Biol Psychiatry 66:320–326.

Hazlett HC, Poe M, Gerig G, Smith RG, Provenzale J, Ross A, Gilmore J, Piven J (2005): Magnetic resonance imaging and head circumference study of brain size in autism: birth through age 2 years. Arch Gen Psychiatry 62:1366–1376.

Herbert MR, Ziegler DA, Deutsch CK, O'Brien LM, Lange N, Bakardjiev A, Hodgson J, Adrien KT, Steele S, Makris N, Kennedy D, Harris GJ, Caviness VS Jr (2003): Dissociations of cerebral cortex, subcortical and cerebral white matter volumes in autistic boys. Brain 126(Pt 5):1182–1192.

Herbert MR, Ziegler DA, Makris N, Filipek PA, Kemper TL, Normandin JJ, Sanders HA, Kennedy DN, Caviness VS Jr (2004): Localization of white matter volume increase in autism and developmental language disorder. Ann Neurol 55:530–540.

Hodge SM, Makris N, Kennedy DN, Caviness VS Jr, Howard J, McGrath L, Steele S, Frazier JA, Tager-Flusberg H, Harris GJ (2010): Cerebellum, language, and cognition in autism and specific language impairment. J Autism Dev Disord 40:300–316.

Hua X, Leow AD, Lee S, Klunder AD, Toga AW, Lepore N, Chou YY, Brun C, Chiang MC, Barysheva M, Jack CR Jr, Bernstein MA, Britson PJ, Ward CP, Whitwell JL, Borowski B, Fleisher AS, Fox NC, Boyes RG, Barnes J, Harvey D, Kornak J, Schuff N, Boreta L, Alexander GE, Weiner MW, Thompson PM, Alzheimer's Disease Neuroimaging Initiative (2008): 3D characterization of brain atrophy in Alzheimer's disease and mild cognitive impairment using tensor-based morphometry. Neuroimage 41:19–34.

Hua X, Leow AD, Levitt JG, Caplan R, Thompson PM, Toga AW (2009): Detecting brain growth patterns in normal children using tensor-based morphometry. Hum Brain Mapp 30:209–219.

Hua X, Leow AD, Parikshak N, Lee S, Chiang MC, Toga AW, Jack CR Jr, Weiner MW, Thompson PM (2008): Tensor-based morphometry as a neuroimaging biomarker for Alzheimer's disease: an MRI study of 676 AD, MCI, and normal subjects-Neuroimage 43:458–469.

Hua X, Hibar DP, Lee S, Toga AW, Jack CR Jr, Weiner MW, Thompson PM (2010): Sex and age differences in atrophic rates: an ADNI study with n=1368 MRI scans. Neurobiol Aging 31:1463–1480.

Hyde KL, Samson F, Evans AC, Mottron L (2010): Neuroanatomical differences in brain areas implicated in perceptual and other core features of autism revealed by cortical thickness analysis and voxel-based morphometry. Hum Brain Mapp 31:556–566.

Just MA, Cherkassky VL, Keller TA, Minshew NJ (2004): Cortical activation and synchronization during sentence comprehension in high-functioning autism: Evidence of underconnectivity. Brain 127:1811–1821.

Just MA, Cherkassky VL, Keller TA, Kana RK, Minshew NJ (2007): Functional and anatomical cortical underconnectivity in autism: Evidence from an FMRI study of an executive function task and corpus callosum morphometry. Cereb Cortex 17:951–961.

Kanner L (1943): Autistic disturbances of affective contact. Nervous Child 2:217–250.

Kates WR, Burnette CP, Eliez S, Strunge LA, Kaplan D, Landa R, Reiss AL, Pearlson GD (2004): Neuroanatomic variation in monozygotic twin pairs discordant for the narrow phenotype for autism. Am J Psychiatry 161:539–546.

Kaufman J, Birmaher B, Brent D, Rao U, Flynn C, Moreci P, Williamson D, Ryan N (1997): Schedule for affective disorders and schizophrenia for school-age children-present and lifetime version (K-SADS-PL): Initial reliability and validity data. J Am Acad Child Adolesc Psychiatry 36:980–988.

Kaufmann WE, Cooper KL, Mostofsky SH, Capone GT, Kates WR, Newschaffer CJ, Bukelis I, Stump MH, Jann AE, Lanham DC (2003): Specificity of cerebellar vermian abnormalities in autism: a quantitative magnetic resonance imaging study. J Child Neurol 18:463–470.

Knickmeyer RC, Gouttard S, Kang C, Evans D, Wilber K, Smith JK, Hamer RM, Lin W, Gerig G, Gilmore JH (2008): A structural MRI study of human brain development from birth to 2 years. J Neurosci 28:12176–12182.

Kochunov P, Lancaster J, Thompson P, Toga AW, Brewer P, Hardies J, Fox P (2002): An optimized individual target brain in the Talairach coordinate system. Neuroimage 17:922–927.

Kochunov P, Lancaster J, Hardies J, Thompson PM, Woods RP, Cody JD, Hale DE, Laird A, Fox PT (2005): Mapping structural differences of the corpus callosum in individuals with 18q deletions using targetless regional spatial normalization. Hum Brain Mapp 24:325–331.

Koshino H, Carpenter PA, Minshew NJ, Cherkassky VL, Keller TA, Just MA (2005): Functional connectivity in an fMRI working memory task in high-functioning autism. NeuroImage 24:810–821.

Kovacevic N, Henderson JT, Chan E, Lifshitz N, Bishop J, Evans AC, Henkelman RM, Chen XJ (2005): A three-dimensional MRI atlas of the mouse brain with estimates of the average and variability. Cereb Cortex 15:639–645.

Le Couteur A, Rutter M, Lord C, Rios P, Robertson S, Holdgrafer M, McLennan J (1989): Autism diagnostic interview: a standardized investigator-based instrument. Journal of autism and developmental disorders 19:363–387.

Leow A, Huang SC, Geng A, Becker JT, Davis S, Toga AW, Thompson PM (2005): Inverse Consistent Mapping in 3D Deformable Image Registration: Its Construction and Statistical Properties. Information Processing in Medical Imaging. Colorado: Glenwood Springs. pp 493–503.

Leow AD, Klunder AD, Jack CR Jr, Toga AW, Dale AM, Bernstein MA, Britson PJ, Gunter JL, Ward CP, Whitwell JL, Borowski BJ, Fleisher AS, Fox NC, Harvey D, Kornak J, Schuff N, Studholme C, Alexander GE, Weiner MW, Thompson PM (2006): Longitudinal stability of MRI for mapping brain change using tensor-based morphometry. Neuroimage 31:627–640.

Levitt JG, Blanton R, Capetillo-Cunliffe L, Guthrie D, Toga A, McCracken JT (1999): Cerebellar vermis lobules VIII-X in autism. Prog Neuropsychopharmacol Biol Psychiatry 23:625–33.

Lord C, Rutter M, DiLavore P, Risi S (1999): Autism Diagnostic Observation Schedule-WPS (WPS Edition). Los Angeles: Western Psychological Services.

Lord C, Rutter M, Le Couteur A (1994): Autism Diagnostic Interview-Revised: a revised version of a diagnostic interview for caregivers of individuals with possible pervasive

developmental disorders. Journal of autism and developmental disorders 24:659–685.

Lord C, Cook EH, Leventhal BL, Amaral DG (2000a): Autism spectrum disorders. Neuron 28:355–363.

Lord C, Risi S, Lambrecht L, Cook EH Jr, Leventhal BL, DiLavore PC, Pickles A, Rutter M (2000b): The autism diagnostic observation schedule-generic: A standard measure of social and communication deficits associated with the spectrum of autism. J Autism Dev Disord 30:205–223.

MacDonald D (1993). Available at: http://www.bic.mni.mcgill.ca/ServicesSoftwareVisualization/HomePage (accessed on September 2011).

Maes F, Collignon A, Vandermeulen D, Marchal G, Suetens P (1997): Multimodality image registration by maximization of mutual information. IEEE Trans Med Imaging 16:187–198.

Mazziotta J, Toga A, Evans A, Fox P, Lancaster J, Zilles K, Woods R, Paus T, Simpson G, Pike B, Holmes C, Collins L, Thompson P, MacDonald D, Iacoboni M, Schormann T, Amunts K, Palomero-Gallagher N, Geyer S, Parsons L, Narr K, Kabani N, Le Goualher G, Boomsma D, Cannon T, Kawashima R, Mazoyer B (2001): A probabilistic atlas and reference system for the human brain: International Consortium for Brain Mapping (ICBM). Philos Trans R Soc Lond B Biol Sci 356, 1293–322.

Mori S, Wakana S, Nagae-Poetscher LM, van Ziji PCM (2005): MRI Atlas of Human White Matter. San Diego, CA: Elsevier Inc.

Morra JH, Tu Z, Apostolova LG, Green AE, Avedissian C, Madsen SK, Parikshak N, Hua X, Toga AW, Jack CR Jr, Weiner MW, Thompson PM (2008): Validation of a fully automated 3D hippocampal segmentation method using subjects with Alzheimer's disease mild cognitive impairment, and elderly controls. Neuroimage 43:59–68.

Nichols TE, Holmes AP (2002): Nonparametric permutation tests for functional neuroimaging: a primer with examples. Hum Brain Mapp 15:1–25.

Piven J, Arndt S, Bailey J, Havercamp S, Andreasen NC, Palmer P (1995): An MRI study of brain size in autism. Am J Psychiatry 152:1145–1149.

Piven J, Arndt S, Bailey J, Andreasen N (1996): Regional brain enlargement in autism: a magnetic resonance imaging study. J Am Acad Child Adolesc Psychiatry 35:530–536.

Rex DE, Ma JQ, Toga AW (2003): The LONI pipeline processing environment. Neuroimage 19:1033–1048.

Riddle WR, Li R, Fitzpatrick JM, DonLevy SC, Dawant BM, Price RR (2004): Characterizing changes in MR images with color-coded Jacobians. Magn Reson Imaging 22:769–777.

Scott JA, Schumann CM, Goodlin-Jones BL, Amaral DG (2009): A comprehensive volumetric analysis of the cerebellum in children and adolescents with autism spectrum disorder. Autism Res 2:246–257.

Seltzer MM, Shattuck P, Abbeduto L, Greenberg JS (2004): Trajectory of development in adolescents and adults with autism. Ment Retard Dev Disabilities Res Rev 10, 234–247.

Shattuck DW, Leahy RM (2002): BrainSuite: an automated cortical surface identification tool. Med Image Anal 6:129–412.

Sivaswamy L, Kumar A, Rajan D, Behen M, Muzik O, Chugani D, Chugani H (2010): A diffusion tensor imaging study of the cerebellar pathways in children with autism spectrum disorder. J Child Neurol 25:1223–1231.

Sled JG, Zijdenbos AP, Evans AC (1998): A nonparametric method for automatic correction of intensity nonuniformity in MRI data. IEEE Trans Med Imaging 17:87–97.

Sowell ER, Thompson PM, Holmes CJ, Batth R, Jernigan TL, Toga AW (1999): Localizing age-related changes in brain structure between childhood and adolescence using statistical parametric mapping. Neuroimage 9:587–597.

Sowell ER, Thompson PM, Leonard CM, Welcome SE, Kan E, Toga AW (2004): Longitudinal mapping of cortical thickness and brain growth in normal children. J Neurosci 24:8223–8231.

Sparks BF, Friedman SD, Shaw DW, Aylward EH, Echelard D, Artru AA, Maravilla KR, Giedd JN, Munson J, Dawson G, Dager SR (2002): Brain structural abnormalities in young children with autism spectrum disorder. Neurology 59:184–192.

Steffenburg S, Gillberg C, Hellgren L, Andersson L, Gillberg IC, Jakobsson G, Bohman M (1989): A twin study of autism in Denmark, Finland, Iceland, Norway and Sweden. J Child Psychol Psychiatry 30:405–416.

Thompson PM, Giedd JN, Woods RP, MacDonald D, Evans AC, Toga AW (2000): Growth patterns in the developing brain detected by using continuum mechanical tensor maps. Nature 404:190–193.

Toga AW (1999): Brain Warping. San Diego: Academic Press. p385.

Webb SJ, Sparks BF, Friedman SD, Shaw DW, Giedd J, Dawson G, Dager SR (2009): Cerebellar vermal volumes and behavioral correlates in children with autism spectrum disorder. Psychiatry Research 172:61–67.

Wechsler D (1991): Wechsler Intelligence Scale for Children-Third Edition. San Antonio, TX: The Psychological Corporation.

Wells WM III, Viola P, Atsumi H, Nakajima S, Kikinis R (1996): Multi-modal volume registration by maximization of mutual information. Med Image Anal 1:35–51.

Wilke M, Schmithorst VJ, Holland SK (2002): Assessment of spatial normalization of whole-brain magnetic resonance images in children. Human Brain Mapping 17:48–60.

Wilke M, Holland SK, Altaye M, Gaser C (2008): Template-O-Matic: A toolbox for creating customized pediatric templates. Neuroimage 41:903–913.

Woods RP, Grafton ST, Watson JD, Sicotte NL, Mazziotta JC (1998): Automated image registration: II. Intersubject validation of linear and nonlinear models. J Comput Assist Tomogr 22:153–165.